Mechanisms for Adsorption of Methyl Viologen on CdS Quantum Dots

Mark D. Peterson, Stephen C. Jensen, David J. Weinberg, and Emily A. Weiss*

Department of Chemistry, Northwestern University, 2145 Sheridan Road, Evanston, Illinois 60208-3113, United States

ABSTRACT This paper describes the surface composition-dependent binding of the dichloride salt of methyl viologen (MV^{2+}) to CdS quantum dots (QDs) enriched, to various degrees, with either Cd or S at the surface. The degree of enrichment is controlled synthetically and by postsynthetic dilution of the QDs in their solvent, THF. NMR shows the Cd-enriched QDs to contain a relatively dense (2.8 ligands/nm^2) surface layer of oleic acid, in the form of Cd-oleate, and S-enriched QDs to contain relatively sparse (1.0 ligands/nm^2) surface density of native ligands containing both oleic acid and octadecene. Electron transfer-mediated photoluminescence quenching of the QDs by MV^{2+} serves as a probe for the binding affinity of MV^{2+} for the surfaces of the QDs. Diluting Cd-enriched QDs removes Cd-oleate from the surface, exposing the stoichiometric CdS surface beneath and increasing the quenching efficiency of MV^{2+}, whereas diluting S-enriched QD does not change their surface chemistry or the efficiency with which they are quenched by MV^{2+}. The photoluminescence quenching data for all of the surface chemistries we studied fit well to a Langmuir model that accounts for binding of MV^{2+} through two reaction mechanisms: (i) direct adsorption of MV^{2+} to exposed stoichiometric CdS surfaces (with an equilibrium adsorption constant of 1.5×10^5 M^{-1}), and (ii) adsorption of MV^{2+} to stoichiometric CdS surfaces upon displacement of weakly bound Cd-oleate complexes (with an equilibrium displacement constant of 3.5×10^3 M^{-1}). *Ab initio* calculations of the binding energy for adsorption of the dichloride salt of MV^{2+} on Cd- and S-terminated surfaces reveal a substantial preference of MV^{2+} for S-terminated lattices due to alignment of the positively charged nitrogens on MV^{2+} with the negatively charged sulfur. These findings suggest a strategy to maximize the adsorption of redox-active molecules in electron transfer-active geometries through synthetic and postsynthetic manipulation of the inorganic surface.

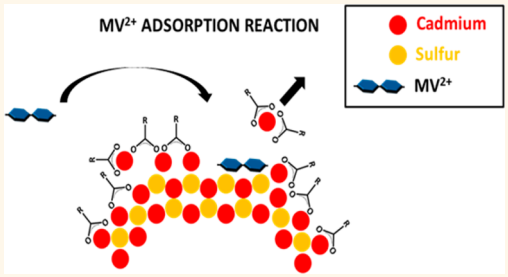

KEYWORDS: cadmium sulfide nanocrystal · enrichment · cadmium oleate complex · Langmuir isotherm · electron transfer · ^{1}H NMR · photoluminescence quenching

This paper describes the mechanisms by which the dichloride salt of methyl viologen (MV^{2+}) molecules adsorb to CdS quantum dots (QDs) in geometries that permit picosecond-time-scale (or faster) photoinduced electron transfer (eT) from the QDs to MV^{2+}. Viologens are an important class of electron acceptors for QDs, with applications as redox shuttles between QD photosensitizers and molecular catalysts,[1−4] and participants in hot electron transfer and multielectron transfer from QDs.[5−7] MV^{2+} does not have an obvious means of coordinating to a QD surface, such as an appended thiol or acid functional group, so the ultrafast rate constants measured reproducibly for photoinduced eT from many types of QDs under a large range of conditions[7−9] imply a single highly coupled donor−acceptor geometry for the QD-MV^{2+} pair that is driven by electrostatic or van der Waals interactions. In previous work, we deduced that the adsorption geometry of a viologen molecule on a CdS QD that leads to ultrafast eT is that where the viologen adsorbs "face-on", such that the bipyridyl core is oriented in a plane parallel to that of the QD surface.[10] This study motivated an interest in the specific interactions that promote complexation of the donor−acceptor pair in this geometry, and whether certain surface chemistries of the QD would promote or inhibit these interactions. This type of mechanistic information is important for achieving picosecond-to-femtosecond hot or multielectron transfer reactions[5,11] involving QDs and viologens (and other molecules without explicit binding groups), because the charge transfer rate between QDs and adsorbed molecular acceptors (i) increases linearly with the number of adsorbed molecules on the QD surface,[9,12] and (ii) increases with the square of the magnitude of the electronic coupling between the donor and acceptor (for nonadiabatic electron transfer (eT) reactions).[13]

* Address correspondence to e-weiss@northwestern.edu.

Received for review December 30, 2013 and accepted February 4, 2014.

Published online February 04, 2014
10.1021/nn406651a

In order to probe the interaction between MV^{2+} and the QD surface that leads to adsorption in the eT-active geometry, we prepared CdS QDs with various surface chemistries, using both synthetic and postsynthetic methods. We synthesized QDs enriched at the surface with either Cd^{2+} or S^{2-} by injecting an excess of the intended terminating ion immediately prior to arresting growth and further manipulated the surface chemistry of these as-prepared samples by simply diluting the QDs with excess solvent (here, THF) and allowing the samples to equilibrate without further purification. X-ray photoelectron spectroscopy (XPS) reveals that dilution of S-enriched QDs does not change the properties of the sample, but progressive dilution of Cd-enriched QDs leads to desorption of Cd-oleate (Cd-OA) from the QD surface[14,15] to reveal the underlying stoichiometric core of the QD. Using eT-mediated photoluminescence (PL) quenching of the QDs by MV^{2+} as a probe, we provide quantitative evidence that MV^{2+} adsorbs to exposed stoichiometric CdS surfaces on all types of QD samples, either directly (with an adsorption constant of 1.5×10^5 M^{-1}), or by displacing weakly bound Cd-OA complexes (with a displacement constant of 3.5×10^3 M^{-1}). We further determine, using *ab initio* calculations, that there is a substantial preference of MV^{2+} for S-terminated stoichiometric surfaces (over Cd-terminated surfaces) due to alignment of the positively charged nitrogens on MV^{2+} with the negatively charged sulfur.

Our findings demonstrate that simple synthetic steps and dilution of as-prepared QD samples can be used to maximize the probability that redox-active molecules will adsorb in an eT-active geometries, even in the absence of a coordinating linker group.

RESULTS AND DISCUSSION

Synthesis of Cd- and S-Enriched Quantum Dots. Most QD synthetic procedures produce cation-enriched surfaces,[14,16−21] because the most tight-binding surfactants in the reaction mixtures are so-called "X-type" (negatively charged) organic ligands that drive cation enrichment of resulting particles.[19,22,23] We synthesize Cd-enriched QDs by heating 0.256 g of CdO, 13.7 mL of octadecene (ODE), and 6.3 mL of oleic acid (OA) to 250 °C under nitrogen in a 3-neck round-bottom flask. Once the CdO completely dissolves and cools to ~60 °C, we place 4 mL into a separate round-bottom flask, add 6 mL of ODE, and heat to 260 °C. To initiate QD growth, we swiftly inject 2 mL of freshly prepared 0.10 M sulfur in ODE and reduce the temperature to 220 °C. After 3 min of growth, we make alternating 0.5-mL additions of Cd and S precursor solutions at ~1 min intervals to promote further growth while preventing ripening. We monitor the progress of the reaction by removing small aliquots from the reaction mixture and acquiring their UV−visible absorption spectra and stop the reaction by removing the heating mantle once the QDs reach the desired size. The solution remains enriched with Cd throughout the entire process, and the final injection contains the Cd precursor to ensure Cd-termination.

It is also possible to produce QDs with anion enriched surfaces.[17,21,24−29] These QDs typically have lower photoluminescence (PL) quantum yields,[17,21,24,25,27−29] shorter exciton lifetimes,[25] and a lower surface coverage of native ligands than cation-enriched lattices.[29] We synthesize S-enriched QDs by heating 42.6 mg of CdO, 14.7 mL of ODE, and 0.3 mL of OA to 300 °C under nitrogen in a 3-neck round-bottom flask. When CdO completely dissolves and the solution turns clear, we swiftly inject 1 mL of freshly prepared 0.15 M sulfur in ODE (prepared by heating elemental sulfur in ODE at <180 °C until completely dissolved, ~20 min) and allow it to react at 250 °C for one hour. To enrich the QDs with sulfur while promoting growth, we add 1.2 mL of 0.15 M S-precursor dropwise over the course of ~10 min until the QDs reach the desired size. We subsequently cooled the reaction mixture to 90 °C for two hours before finally cooling to room temperature.

We purify both types of QDs by extraction with a 3:1 volume addition of methanol:QDs and ~1 mL of butanol to encourage mixing. The mixture is shaken vigorously and spun in a centrifuge at 3500 rpm for 5 min. After removing the nonsolvent phase, we add another ~2 mL of THF and enough acetone to precipitate the QDs. Centrifugation and decantation separates the QDs from the supernatant, and we repeat the washing step with acetone once more. Finally, we resuspend the QD pellet in THF to create a solution with an optical density of ~1 AU at the band-edge in a 1-cm cuvette. Representative transmission electron microscopy images of the Cd- and S-enriched samples are provided in Figure S1 of the Supporting Information.

Figure 1A shows the ground state absorption spectra of Cd- and S-enriched CdS QDs in THF. The first excitonic feature of the absorption spectrum of both Cd- and S-enriched QDs occurs at 443 nm, corresponding to an average diameter of 5.0 nm as calculated from published sizing curves.[30] The first excitonic peak in S-enriched QDs is broader than those in Cd-enriched QDs, consistent with previous results.[27] Our inability to resolve the second excitonic peak in the absorption spectrum of S-enriched QDs suggests that the size distribution of QDs is more heterogeneous than in the Cd-enriched QD sample.

Figure 1B shows the PL spectra of Cd- and S-enriched CdS QDs in THF. The emission spectrum for the Cd-enriched QDs is typical of this lattice termination[27] and includes two major features corresponding to emission from the band-edge exciton and trapped exciton (where one or both carriers are trapped in a localized defect site), respectively; we refer to the emission from a trapped exciton as "defect emission". The band-edge emission is centered at 453 nm and has a full-width-at-half-max (FWHM) of 19 nm, corresponding

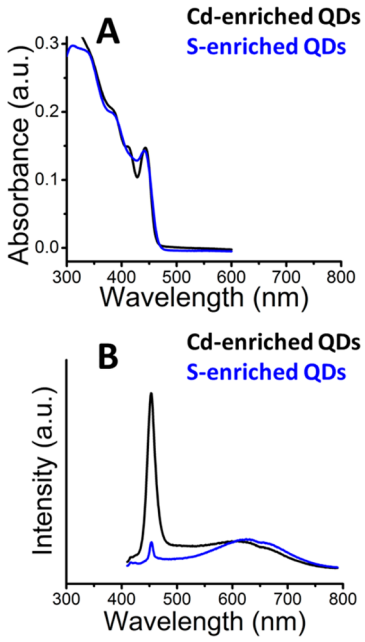

Figure 1. (A) Ground state absorption spectra of CdS QDs enriched with either Cd ("Cd-enriched", black, 6.9 × 10^{-7} M) or S ("S-enriched", blue, 6.8 × 10^{-7} M), in THF. The first excitonic peak is at λ = 443 nm for both samples; this energy corresponds to a core diameter of 5.0 nm. (B) Photoluminescence spectra of the same samples of QDs, excited at 400 nm, showing the relative contribution of band-edge (453 nm) and "defect" (~630 nm, broad) emission in Cd- and S-enriched QDs. The integrated intensity of the band-edge emission in the S-enriched QDs is ~5% of that in the Cd-enriched QDs, and the integrated intensity of the defect emission is approximately the same in the two types of QDs.

to a size dispersity of ~8%. The width of the defect emission peak, centered at ~630 nm, is typically interpreted as a reflection of the distribution of hole trap state energies within the band gap,[31,32] or of the distribution of vibronic modes with which a charge carrier couples.[33,34] Figure 1B also shows the PL spectrum of S-enriched CdS QDs in THF. This spectrum has the same features from band-edge emission and defect emission as the spectrum of Cd-enriched QDs, but the band-edge emission is quenched by ~95% on going from Cd- to S-enrichment. This observation suggests that sulfur termination creates states in which at least one excitonic charge carrier, almost certainly the excitonic hole,[27,35−37] localizes, and that the time constant for this localization process is much shorter than that for band-edge radiative decay, which has a lifetime of ~40 ns.[12] The intensity of the defect emission peak at ~630 nm appears to be insensitive to the termination scheme; therefore, (i) the localized states created by sulfur termination are *not* the trap states that contribute to defect emission, and (ii) defect emission probably originates from recombination of a band-edge carrier and a carrier trapped within the lattice of the QD core. Many previous papers have shown that the trapped carrier in this scenario is the hole.[27,35−37]

Characterization of the Inorganic/Organic Interfaces of Cd- and S-Enriched QDs. Figure 2A,B shows the $Cd_{5/2}$ and $Cd_{3/2}$ peaks within the XPS spectra of Cd-enriched (A) and S-enriched (B) CdS QDs dropcast from THF onto a Si/SiO_2 wafer. The $Cd_{3/2}$ and $Cd_{5/2}$ peaks appear at ~404 and ~410 eV, respectively, in agreement with previous reports.[38,39] Each of the Cd peaks is fit to a sum of two Gaussian functions; the low energy component of each peak reflects the fully coordinated Cd^{2+} within the QD core and surface Cd^{2+} that is well-passivated by OA (see Section 2 in the Supporting Information for the XPS spectrum of molecular Cd-stearate complexes).[27] The high-energy component of each peak corresponds to surface Cd^{2+} that is undercoordinated, either because it is bare or incompletely passivated by OA. The contribution of the unpassivated Cd peaks, relative to the passivated Cd peaks, is greater in the spectrum of Cd-enriched QDs than in the spectrum of S-enriched QDs, consistent with our intended lattice termination scheme; however, S-enriched QDs do contain a small portion of unpassivated Cd suggesting some exposed stoichiometric CdS surfaces or Cd-OA complexes.

Figure 2C,D shows the sulfur peaks within the XPS spectra of Cd-enriched (C) and S-enriched (D) CdS QDs. The spectra of both types of QDs contain three major contributions: passivated $S_{1/2}$, passivated $S_{3/2}$, and unpassivated S,[38,40] where the individual contributions from $S_{1/2}$ and $S_{3/2}$ in unpassivated sulfur cannot be resolved. Passivated sulfur is either in the core of the QD or is coordinated by ligands at the surface of the QD. Unpassivated sulfur is surface sulfur that is undercoordinated and oxidized;[39] several reports show that the oxidized sulfur at 168 eV corresponds to $CdSO_4$.[39,41,42] The appearance of oxidized sulfur peaks in these spectra is not necessarily indicative of oxidation of the sulfur in the QD sample we study with optical and NMR spectroscopy, because a vast majority of this oxidation probably occurs in the few minutes that the XPS sample is exposed to air upon transfer into the XPS chamber. The presence of oxidized sulfur peaks in the XPS spectra simply implies that incompletely passivated sulfur (sulfur vulnerable to oxidation) is present in the solution-phase samples. The greater fractional contribution of unpassivated sulfur to the XPS spectrum of S-enriched QDs, relative to Cd-enriched QDs, is consistent with the intended lattice termination scheme. Tables S1 and S2 in the Supporting Information lists the peak positions, areas, widths, and assignments for the XPS spectra shown in Figure 2.

As an independent confirmation of the surface enrichment suggested by the XPS data, we attempted to quantify the concentrations of Cd and S in our samples using inductively coupled plasma atomic emission spectroscopy (ICP-AES). In a representative experiment, we calculated a Cd-to-S ratio of 1.3:1 for Cd-enriched QDs and 0.5:1 for S-enriched QDs. This method, however, is notoriously inaccurate for measuring sulfur concentrations, so while our results are

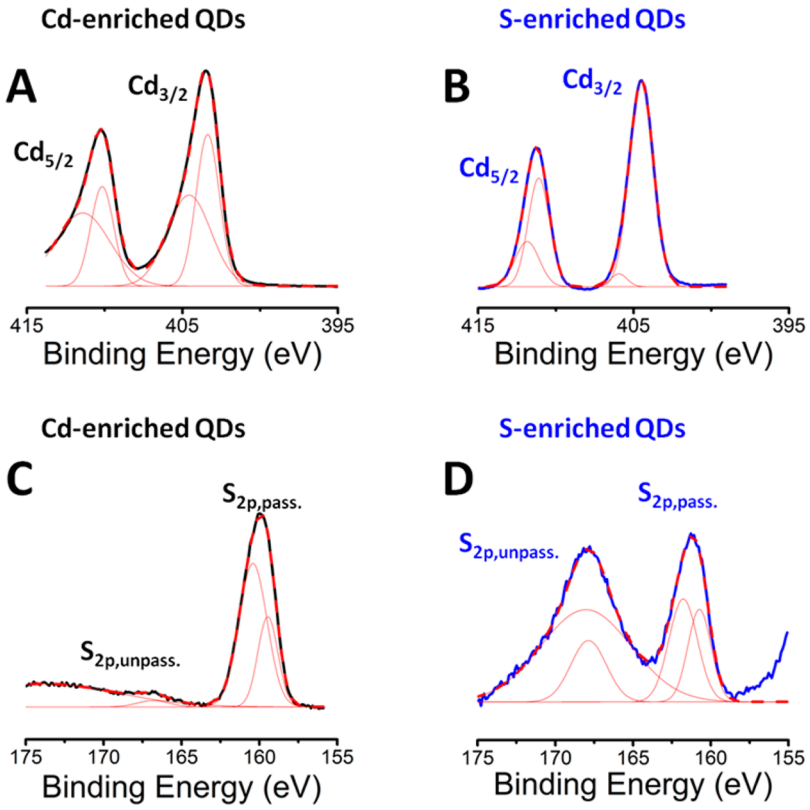

Figure 2. $Cd_{5/2}$, $Cd_{3/2}$, and S_{2p} regions of the XPS spectra of Cd- and S-enriched CdS QDs, as-prepared (before dilution), dropcast from THF onto a Si/SiO_2 wafer. The $Cd_{3/2}$ and $Cd_{5/2}$ peaks of Cd-enriched QDs (A) and S-enriched QDs (B) each fit to a sum of two Gaussians, corresponding to Cd within the QD core (low energy) and excess, unpassivated surface Cd (high energy). The S peaks of Cd-enriched QDs (C) are fit to a sum of two Gaussians corresponding to $S_{1/2}$ (158.5 eV) and $S_{3/2}$ (160.4 eV) electrons of sulfur ions in the QD core or sulfur ions that are well-passivated by ligands on the QD surface. The S peaks within S-enriched QDs (D) are also fit to a sum of two Gaussians corresponding to $S_{1/2}$ (160.8 eV) and $S_{3/2}$ (161.8 eV) electrons of sulfur ions in the QD core or sulfur ions that are well-passivated by ligands on the QD surface. The peak at 168 eV in (D) corresponds to $CdSO_4$, and the broadest high energy peak is required to fit the background. Table S1 in the Supporting Information summarizes all of the peak parameters and assignments for these spectra.

qualitatively consistent with the expected Cd- and S-enrichment scheme, we do not use the ICP-AES numbers in any quantitative conclusions we make about the system.

Figure 3 shows the vinylic region of the ^1H NMR spectra of the Cd- and S-enriched QDs and, for reference, spectra of neat OA and ODE, the two surfactants used in the syntheses of the QDs. The spectra are normalized to the largest peak within the region of 4.5 to 6.0 ppm and offset along the *y*-axis for clarity. In order to remove any excess surfactant, in addition to washing the QD samples with acetone and methanol (as described in the synthetic procedure above), we cleaned the samples for NMR by evaporating the solvent, rinsing the QD solid five times with methanol and five times with acetone, drying under a vacuum for one hour, and redispersing the QDs in $CDCl_3$. We measured the concentrations of the OA and ODE ligands by integrating the peak at 5.3 ppm, corresponding to protons on the internal double bond of OA, and the triplet peak at 5.0 ppm, corresponding to protons on the terminal double bond of ODE, and comparing those integrated intensities to that of a biphenyl integration standard added in known concentration (see Supporting Information, Figure S3). Cd-enriched QDs are coated exclusively with OA, with a total ligand density of 2.8 ligands/nm^2 (~38% of total surface sites, see Section 6 in the Supporting Information). S-enriched QDs are coated with ODE (15%) and OA (85%), with a lower total ligand density of 1.0 ligands/nm^2 (~14% of total surface sites). The reduced overall ligand density for the S-enriched QDs is consistent with previous reports on anion enriched QDs[29] and results in part from the lower surface coverage of Cd^{2+}, which is the ion to which OA binds.

MV^{2+} Quenches S-Enriched QDs More Efficiently than It Quenches Cd-Enriched QDs. Figure 4A shows the quenching of the PL intensities of Cd- and S-enriched QDs ([QDs] = 1×10^{-6} M) upon exposure to increasing concentrations of MV^{2+}. Increasing the molar ratio MV^{2+}:QD within a mixture decreases the PL intensity of the ensemble of QDs because eT from the QD to MV^{2+} forms a nonradiative ion pair. We divide the observed integrated PL intensity of the QDs at each concentration of added MV^{2+} by the integrated intensity of the "blank" (no added MV^{2+}) to get the ratio

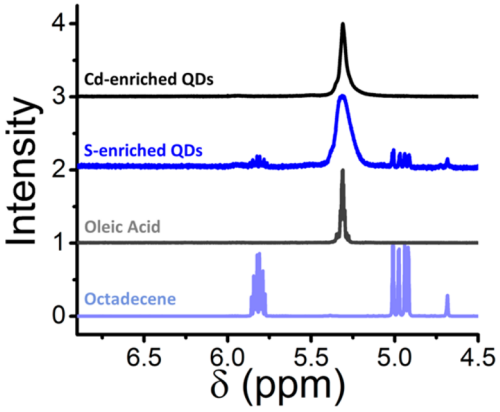

Figure 3. ^{1}H NMR spectra of Cd-enriched QDs (black), S-enriched QDs (blue), neat OA (gray), and neat ODE (light blue) in $CDCl_3$, scaled and offset along the *y*-axis for ease of comparison. Figure S3 in the Supporting Information contains complete spectra of the Cd- and S-enriched QDs normalized to the intensity of a peak corresponding to a biphenyl standard. The spectrum of the Cd-enriched QDs (black) includes a peak at 5.3 ppm corresponding to the olefinic protons of OA. S-enriched QDs show peaks corresponding to the olefinic protons of OA (5.3 ppm) and to ODE [4.7, 5.0 (terminal protons on primary carbon), and 5.8 ppm (terminal proton on secondary carbon)].

PL/PL_0 and plot PL/PL_0 against the concentration of MV^{2+} in Figure 4B. A description of how we correct for the contribution of MV^{2+} to the total PL intensity is provided in Section 8 of the Supporting Information. Figure 4B shows that at this concentration of QDs (1×10^{-6} M) and any given molar ratio MV^{2+}:QD, the PL intensity of S-enriched QDs is more quenched than that of Cd-enriched QDs.

The observed difference in quenching efficiency could be due to either a difference in the intrinsic (single donor−single acceptor) electron transfer rate, $k_{CS,int}$, or a difference in the binding affinity of MV^{2+} for the QD surface in the eT-active "face-on" geometry, since the probability of quenching by eT increases with the number of adsorbed MV^{2+} acceptors per QD. We use a statistical model, described in detail elsewhere[9,43] and in Section 5 of the Supporting Information, to deconvolute these two factors. This model utilizes two assumptions: (i) the number of adsorbed MV^{2+} molecules per QD is Poisson-distributed,[44,45] and (ii) the rate of eT from the QD to MV^{2+} is fast enough such that, if at least one MV^{2+} is adsorbed on a QD in an eT-active geometry, eT occurs with 100% quantum yield.[9] Assumption (i) has been verified in a number of previous studies by us[9,43] and others.[44] We verify assumption (ii) by fitting of kinetic traces for electron decay in Cd- and S-enriched QDs with and without added MV^{2+}, measured with ultrafast TA spectroscopy, with a sum of simple exponential functions. These fits show that the fastest electron decay process occurs in ~500 ps in the absence of MV^{2+} (see Figure S4 in the Supporting Information), while the charge separation process (formation of MV^{1+}) occurs with a time constant of ~50 ps (see Figure 4C). Assumption (ii) is therefore reasonable for this system.

We obtain the intrinsic charge separation rate constant, $k_{CS,int}$ for the QD-MV^{2+} donor−acceptor pair for Cd- and S-enriched QDs by fitting the distributed dynamics of the formation of MV^{1+} within QD-MV^{2+} mixtures with the Poisson model. The fitting procedure and results are described in detail in Section 5 of the Supporting Information. The value of $k_{CS,int}$ for the Cd-enriched QDs (2.3×10^{10} s^{-1}) is, in fact, larger, but only slightly larger (by a factor of 1.6) than that for the S-enriched QDs (1.4×10^{10} s^{-1}). This result implies that (i) the increased quenching efficiency of MV^{2+} on S-enriched QDs stems from preferential adsorption of MV^{2+} onto the S-enriched QD surface, not a faster charge separation process in the S-enriched QDs; and (ii) the adsorption geometry for MV^{2+} molecules that participate in eT is approximately the same for Cd-enriched and S-enriched QDs. Different adsorption geometries would lead to very different rate constants for eT in the two systems, which we do not observe. We note that in measuring the ratio PL/PL_0, we are only investigating the binding of MV^{2+} to the emissive subpopulation of the QD ensemble, and that our analysis assumes that MV^{2+} binds with the same affinity to emissive and nonemissive QDs.

Tuning the Surface Coverage of MV^{2+} with the Surface Chemistry of the QD. The PL quenching curves (Figure 4B) and the charge separation dynamics (Figure 4C) together suggest that the geometry of the QD-MV^{2+} donor−acceptor pair, and the chemical structure of the surface site onto which MV^{2+} adsorbs, is the same in Cd-enriched and S-enriched QDs, but that these surface sites are more accessible in the S-enriched sample than in the Cd-enriched sample. Both Cd-enriched and S-enriched QDs have stoichiometric CdS surfaces (some Cd-terminated, some S-terminated, depending on the crystal face) underneath the more disordered layers of surface ions and accompanying ligands. The Cd- and S-enrichment processes probably do not, in general, produce perfectly continuous shells of the enriching ion but rather patchy layers that leave sections of the core exposed. A MV^{2+} adsorbed to an exposed section of the stoichiometric CdS core is most likely to participate in ultrafast eT with the excitonic electron. We therefore hypothesized that the eT-active MV^{2+} adsorbs to a stoichiometric surface, either by displacing an organic complex of the enriching ion, or directly. In this case, the surfaces of S-enriched QDs either contain more of these exposed stoichiometric surface sites or are more vulnerable to displacement of surface ions by MV^{2+}.

In order to investigate this hypothesis, we manipulated the surface chemistry of the QDs further by simply diluting the QD/MV^{2+} system. We[19,23] and others[46] have shown previously that cadmium enrichment in CdX QDs is in the form of weakly adsorbed complexes of cadmium and negatively charged

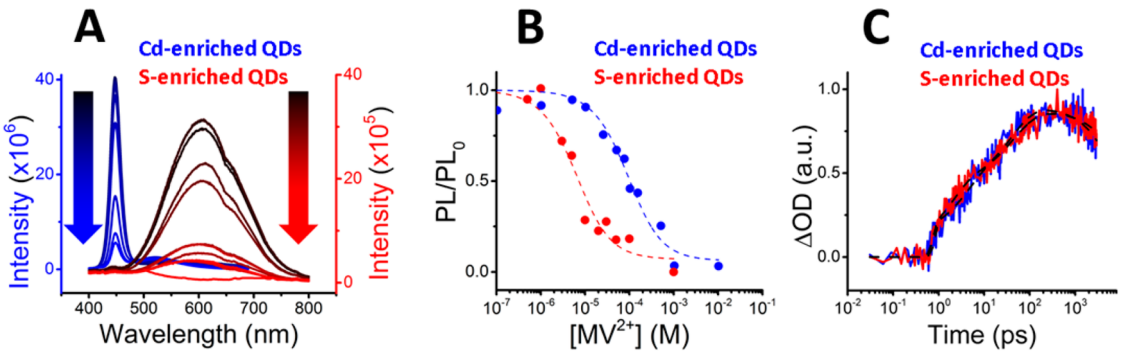

Figure 4. (A) PL spectra for 1×10^{-6} M Cd-enriched QDs (blue, left axis) and S-enriched QDs (red, right axis) in THF upon exposure to increasing concentrations of MV^{2+} (as indicated by the arrows). (B) The PL intensity of each sample of QDs with added MV^{2+} divided by the PL intensity of the QDs in the absence of MV^{2+}, PL/PL_0, plotted against the concentration of added MV^{2+}. Fits correspond to the two-reaction Langmuir model (eq 1) described in the text. (C) Kinetic traces, measured with TA, showing the growth of the MV^{1+} transient at 620 nm (see Figure S5, and fit to the distributed rate model outlined in Section 5 of the Supporting Information). The intrinsic (single donor−single acceptor) rate constants for charge separation, $k_{CS,int}$, from the Cd- and S-enriched QDs to MV^{2+} are within a factor of 1.6 of each other.

"X-type" ligands, here oleate, and that in the absence of a proton donor excess Cd desorbs as Cd-OA complexes to reveal a stoichiometric lattice. Figure 5A shows the sulfur 2p peaks within normalized XPS spectra of Cd-enriched QDs at three concentrations; the spectrum of the most concentrated sample is identical to that in Figure 2C. As the initially Cd-enriched QDs are diluted in THF, the surface coverage of well-passivated sulfur (160 eV) decreases until only unpassivated sulfur (168 eV) is observed (we suspect that we do not observe signal from sulfur in the core of the QD because the XPS signal is dominated by surface atoms).[38] The transformation of passivated sulfur to unpassivated sulfur upon dilution of the Cd-enriched QDs is consistent with desorption of Cd-OA from the QD surface in the absence of any passivating ligands for sulfur; OA is the only ligand present in these samples, Figure 3. The left-most column of Scheme 1A,B shows the surface chemistries of the initially Cd-enriched QDs (at 1×10^{-6} M) and the Cd-enriched QDs upon dilution to 2×10^{-8} M that is consistent with our NMR and XPS studies.[15]

Figure 5A also shows Langmuir binding isotherms for MV^{2+}-QD complexes, for the same three samples of initially Cd-enriched QDs analyzed in the corresponding XPS spectra. We calculate the fractional surface coverage of MV^{2+} on the QD, θ, and the concentration of unbound MV^{2+}, $[MV^{2+}]_{free}$, in each QD-MV^{2+} mixture with the Poisson model described above. Within this model, the average number of adsorbed MV^{2+} per QD, λ, equals $-\ln(PL/PL_0)$ for each concentration of added MV^{2+}.[9] The fractional surface coverage of MV^{2+} on the QD, θ, is then λ divided by the total number of surface sites per QD, N ($\theta = \lambda/N$). We estimate N using geometric considerations, as described in Section 6 of the Supporting Information. Then, $[MV^{2+}]_{free} = [MV^{2+}]_{total} - \lambda[QD]$. These isotherms show that the affinity of MV^{2+} for surfaces of initially Cd-enriched QDs increases as the concentration of the QDs decreases from 1×10^{-6} to 2×10^{-8} M; this result is consistent with our hypothesis that dilution results in desorption of Cd-OA and exposure of the stoichiometric CdS surface, to which the MV^{2+} binds in its eT-active configuration.

Figure 5B shows that, in contrast with the Cd-enriched samples, the surfaces of S-enriched QDs are stable to dilution in THF in this concentration range. The surfaces of these QDs contain a mix of well-passivated and incompletely passivated sulfur (160 and 168 eV). Our work with PbS QDs[47] suggests that the ODE is transiently bound to the QD either as covalent alkyl-thiolate complexes, formed by the reaction of ODE with elemental sulfur at elevated temperatures and resulting in the migration of the double bond,[48,49] or as datively bound ODE/Cd^{2+} complexes. The left-most column of Scheme 1C illustrates the surface chemistry of S-enriched QDs that is consistent with our NMR and XPS studies. Figure 5B also shows that the surface coverage (θ) of MV^{2+} on S-enriched QD does not vary with dilution of the QDs in this range, consistent with the stability of the S-enriched surface evident in the XPS spectra. We could not obtain PL/PL_0 plots of S-enriched QDs for the most dilute samples of S-enriched QDs (2×10^{-8} M) because the PL intensities were too low to integrate the peaks accurately.

Given the data in Figures 4 and 5, and our knowledge of the interfacial structures of the QDs, as shown in Scheme 1 (left column), we propose that there are two mechanisms by which MV^{2+} adsorbs to the surfaces of CdS QDs in the eT-active "face-on" geometry: (i) by displacing Cd-OA complexes from the surface and then adsorbing to the exposed stoichiometric CdS surface, or (ii) by adsorbing directly to an already exposed stoichiometric CdS surface. We assign the displacement reaction an equilibrium constant $K_{a,1}$, and we assign the direct adsorption reaction an equilibrium constant $K_{a,2}$, such that $K_{a,1} = K_{a,2}/K_{a,Cd\text{-}OA}$. Scheme 1 (right column) illustrates these mechanisms.

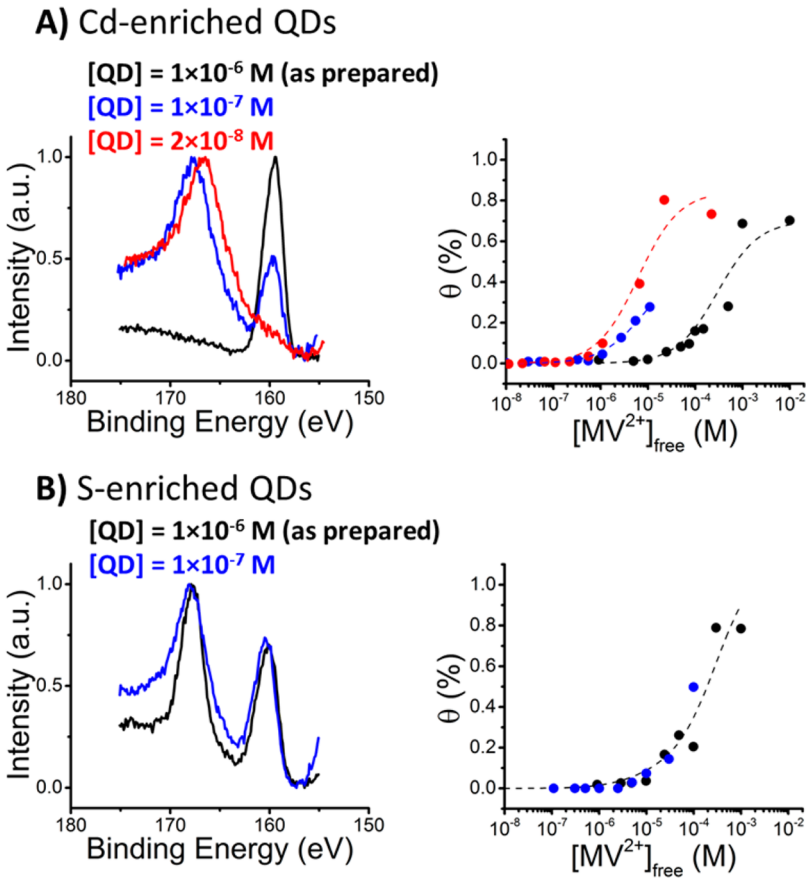

Figure 5. (A) Left: Normalized XPS spectra of S regions of Cd-enriched QDs at various concentrations. As the concentration of Cd-enriched QDs decreases from 1×10^{-6} M to 2×10^{-8} M, we observe a decrease in the ratio of passivated S (160 eV) to unpassivated S (168 eV), which corresponds to the oxidization of surface sulfur exposed upon desorption of Cd-OA. Right: PL/PL_0 is used to calculate θ, as described in the main text, which is plotted, as a percentage surface coverage, against the concentration of free MV^{2+} and fit to a Langmuir isotherm modified to reflect binding through two distinct reactions; the results are summarized in Table 1. Dilution of Cd-enriched QDs leads to an increase in quenching efficiency by MV^{2+} due to desorption of native ligands and surface reconstruction. (B) Left: XPS spectra of S regions of S-enriched QDs at various concentrations. The oxidation state of S within as-prepared S-enriched QDs changes minimally upon dilution of the QDs. That we observe a nonzero peak at 160 eV in spectra reflecting S-enriched QDs suggests that these samples are not completely S-enriched. Right: S-enriched QDs maintain similar quenching curves upon dilution.

This simple model suggests that we fit the isotherms in Figure 5 with a Langmuir function for binding of MV^{2+} *via* two possible reactions,[50,51] eq 1,

$$\theta = \frac{\lambda}{N} = \theta_{1,\max}\frac{K_{a,1}[MV^{2+}]_{free}}{(1 + K_{a,1}[MV^{2+}]_{free})} + \theta_{2,\max}\frac{K_{a,2}[MV^{2+}]_{free}}{(1 + K_{a,2}[MV^{2+}]_{free})} \quad (1)$$

where $K_{a,X}$ is the equilibrium constant for adsorption of MV^{2+} to the QD *via* reaction *X*, and $\theta_{X,\max}$ is the maximum fractional surface coverage MV^{2+} can achieve through reaction *X*. The four fitting parameters are $K_{a,1}$, $K_{a,2}$, $\theta_{1,\max}$, and $\theta_{2,\max}$. We constrain the fit by sharing the values of $K_{a,1}$ and $K_{a,2}$ across all five data sets in Figure 5, because, within this model, the same adsorption and displacement processes are happening in each sample but to different degrees. Table 1 shows the results of the fits of the data in Figure 5A,B to eq 1. A few notes about the use of eq 1: (i) Although our model is probably not the only model that will fit these data, the fit we obtain with eq 1 is rigorous and unique; that is, the result of the fit does not depend on the initial guess values of our fitting parameters. Figure S6 in the Supporting Information shows that the data does not fit to a Langmuir isotherm with one adsorption constant shared among all of the data sets, even when we omit the data set for the 1×10^{-6} M Cd-enriched QDs, which are most different in their surface chemistry from the rest of the samples. (ii) This model only accounts for MV^{2+} adsorbed in eT-active geometries. For instance, it is conceivable that a MV^{2+} molecule will physisorb to sulfur within one of the sulfur-enriched regions of the QD surface; but, if this adsorption geometry does not lead to ultrafast eT, the PL/PL_0 measurement that we use to measure surface coverage will not detect it. The satisfactory fit of the data to this two-reaction Langmuir with shared values of K_a for both Cd-enriched and S-enriched samples implies that the two adsorption mechanisms we outline in Scheme 1 are adequate to describe this system.

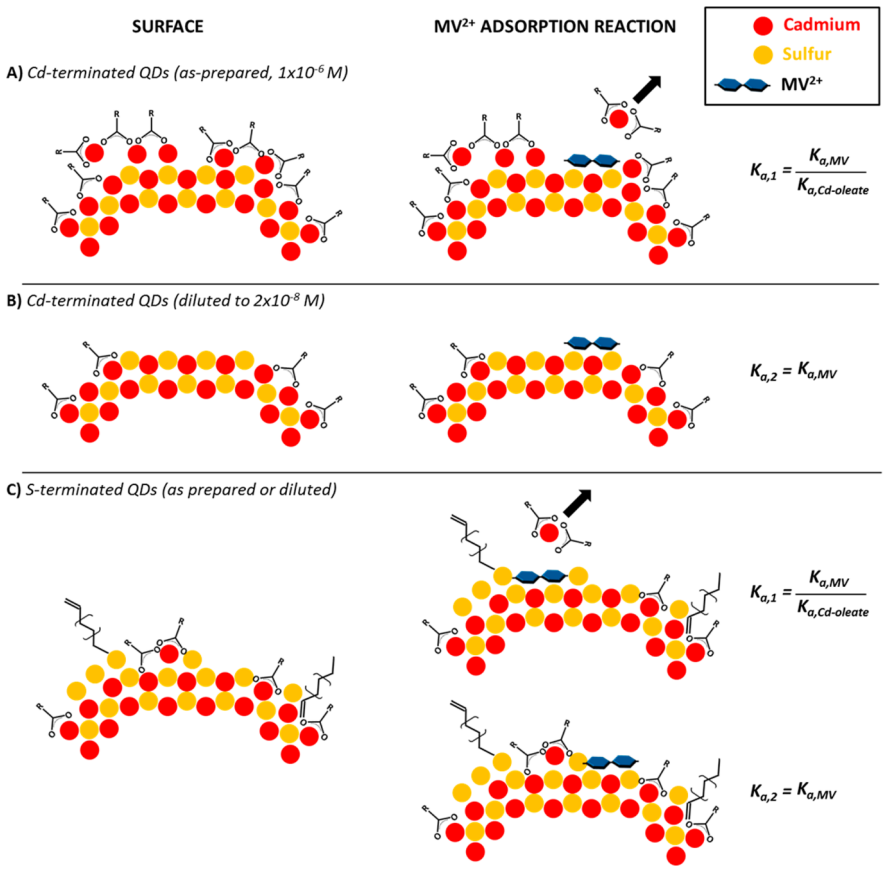

Scheme 1. (A) Left: Schematic diagram of the cross-section of 1×10^{-6} M Cd-enriched QDs (as prepared), showing the excess surface Cd in the form of Cd-OA complexes, and complete passivation of sulfur ions, as measured by XPS. Right: Displacement of weakly-bound Cd-OA complexes by MV^{2+} with equilibrium constant $K_{a,1}$. (B) Left: Loosely bound Cd-OA species desorb upon dilution of the initially Cd-enriched QDs to reveal exposed stoichiometric surfaces consistent with the unpassivated sulfur detected by the XPS measurements. Right: Direct adsorption of MV^{2+} onto stoichiometric CdS surfaces exposed upon dilution of the QDs, with equilibrium constant $K_{a,2}$. (C) Left: As prepared S-enriched QDs have both OA and ODE ligands, where the ODE ligands may coordinate covalently to surface S to produce an alkyl-thiol adduct, resulting in the migration of the double bond, or datively to under-coordinated surface Cd. Both passivated and unpassivated sulfur is present, and these surfaces do not change with dilution. Right: MV^{2+} binds to S-enriched QDs through a combination of direct adsorption and displacement of Cd-OA. We have omitted the chloride counterions for MV^{2+} for clarity, but their positions, and a more precise diagram of the most favorable orientations of MV^{2+} on the stoichiometric surfaces is shown in Figure 6. The diagrams in the figure are not to scale.

TABLE 1. Summary of the Fits of the Data in Figure 5A,B to eq 1

surface chemistry (as-prepared)[a]	concentration of QDs	$K_{a,1}$[c] (M^{-1})	$K_{a,2}$[c] (M^{-1})	$\theta_{1,max}$	$\theta_{2,max}$
Cd-enriched	1×10^{-6} M	3.5×10^{3}	1.5×10^{5}	7.1×10^{-3}	0
Cd-enriched[b]	1×10^{-7} M	3.5×10^{3}	1.5×10^{5}	7.8×10^{-3}	4.1×10^{-3}
Cd-enriched[b]	2×10^{-8} M	3.5×10^{3}	1.5×10^{5}	0	8.9×10^{-3}
S-enriched	1×10^{-6} M	3.5×10^{3}	1.5×10^{5}	1.0×10^{-2}	8.9×10^{-4}
S-enriched[b]	1×10^{-7} M	3.5×10^{3}	1.5×10^{5}	1.0×10^{-2}	8.9×10^{-4}

[a] Surface chemistry of the QDs after purification and before their dilution to the indicated concentrations. [b] Diluted to the indicated concentration in THF. [c] Globally fit parameters: values shared among all five samples.

From the values of the fitting parameters in Table 1, we conclude the following: (i) The equilibrium constant for direct adsorption of MV^{2+} onto the stoichiometric CdS surface ($K_{a,2} = 1.5 \times 10^{5}$ M^{-1}) is approximately a factor of 50 higher than that for MV^{2+} binding through displacement of Cd-OA ($K_{a,1} = 3.5 \times 10^{3}$ M^{-1}). This result implies that $K_{a,Cd\text{-}OA}$ is approximately 50 M^{-1}. Uncertainty in the values of θ and $[MV^{2+}]_{free}$ leads to uncertainty in K_a. The largest uncertainty in θ arises at small values of PL/PL_0, where the PL signal may be difficult to distinguish from the background; however, small values of PL/PL_0 generate large values of θ, so low PL intensities lead to large error in θ_{max} but small error in K_a. (ii) The fit yields $\theta_{1,max} = 0$ for the most dilute (2×10^{-8} M) Cd-enriched QDs (meaning that no displacement of Cd-OA is required for MV^{2+} to adsorb these surfaces), and $\theta_{2,max} = 0$ for the most concentrated (1×10^{-6} M) Cd-enriched QDs (meaning that

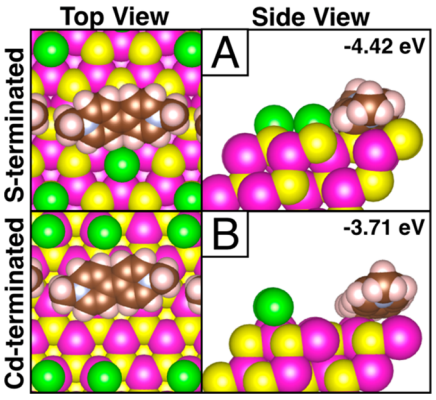

Figure 6. The most stable binding geometry of MV^{2+} on S-terminated QDs (A, top panels) and Cd-terminated QDs (B, bottom panels). The stabilization energy associated with binding of MV^{2+} is more favorable with S-terminated QDs than Cd-terminated QDs because of the stabilizing interaction of S^{2-} with the N^{+} in the bipyridyl core. The atoms are color-coded as follows: Cd, purple; S, yellow; Cl, green; C, brown; H, gray.

adsorption of MV^{2+} to these surfaces *only* occurs through displacement of Cd-OA). For the intermediate concentration of Cd-enriched QDs, and for both samples of as prepared S-enriched QDs, MV^{2+} binds to the QDs both directly and through Cd-OA desorption. (iii) $\theta_{X,max}$, the maximum fractional surface coverage of MV^{2+} achievable through each adsorption mechanism, is not conserved upon dilution; for instance, desorption of Cd-OA upon dilution to 1×10^{-7} M appears to destabilize other Cd-OA groups on the QD surface such that they can eventually be displaced by MV^{2+}. We should not, however, interpret the values of $\theta_{1,max}$ and $\theta_{2,max}$ too strictly because, as discussed above, the uncertainty in $\theta_{X,max}$ is relatively large when the PL intensity is difficult to deconvolute from the noise.

Calculation of the Preferred Orientation of MV^{2+} on a Stoichiometric CdS Surface. We have so far concluded that eT-active MV^{2+} molecules adsorb to stoichiometric CdS surfaces through one of two mechanisms. We use density functional theory (DFT) calculations, performed with the Vienna *Ab Initio* Simulation Package (VASP) (version 5.3) within MedeA software (Materials Design), to determine which intermolecular interactions drive this adsorption, and which orientation of MV^{2+} on the CdS surface is optimal. We calculated the adsorption energies of MV^{2+} on the most thermodynamically stable facet, (0001), of wurtzite Cd- and S-terminated CdS stoichiometric lattices. Section 9 of the Supporting Information contains details of the simulation. The surface was created using $(CdS)_{24}$ in a $(4 \times 3 \times 4)$ unit cell configuration with the same bulk structure for both the Cd- and S-terminated surfaces. We held the bulk coordinates for the bottom half of the structure constant and allowed the structure of either the Cd- or S-terminated half to relax. The bottommost layer of the sample is terminated with hydrogen to quench gap states caused by under-coordination. We added MV^{2+} to these surfaces as a dichloride salt (as we do in the experiment), and calculated the adsorption energy for the MV^{2+}/CdS system by subtracting the energy of the lattice and MV^{2+}, physically separated in a vacuum, from the energy of the lattice with MV^{2+} and two chloride ions adsorbed to the surface, eq 2.

$$E_{ads} = E_{surface+MV^{2+}+2Cl^{-}} - (E_{surface} + E_{MV^{2+}+2Cl^{-}}) \quad (2)$$

In the most stable configurations calculated, the magnitude of E_{ads} is larger for S-terminated lattices (−4.42 eV) than for Cd-terminated lattices (−3.71 eV).

Figure 6 shows the preferred orientation of MV^{2+} and associated chloride ions on a S-terminated surface (Figure 6A) and a Cd-terminated surface (Figure 6B). The lowest energy conformation of MV^{2+} on both Cd- and S-terminated QDs is a "face-on" geometry, as expected from our previous work,[10] with the plane of the bipyridyl core parallel to the particle surface. On S-terminated surfaces, the nitrogens in MV^{2+} both lie directly above surface sulfurs at distances of 3.2 and 3.3 Å (Figure 6A). The chloride counterion preferentially adsorbs adjacent to the MV^{2+} at an $H-Cl^{-}$ bond distance of 2.6 Å. On Cd-terminated QDs, the preferred binding geometry involves one nitrogen above S^{2-} in the surface layer, with a N−S bond distance of 3.8 Å, and another above a Cd^{2+} at a much larger distance of 4.8 Å. The distance between a hydrogen in MV^{2+} and the surface chloride is 3.3 Å.

Other, less stable orientations and their corresponding energies are shown in Figures S7 and S8 in the Supporting Information. For S-terminated surfaces, rotation of MV^{2+} within the plane of the surface only weakly perturbs the stabilization energy, but the destabilization energy associated with rotating the MV^{2+} perpendicular to the nanoparticle surface is up to 0.69 eV. For Cd-terminated surfaces, rotation of MV^{2+} within the surface plane causes a weak to modest perturbation in the stabilization energy, and rotation of MV^{2+} perpendicular to the surface causes a modest destabilization of 0.19 eV. These calculations suggest that the preferential binding of MV^{2+} to S-terminated surfaces results primarily from the stabilization energy gained by orienting the positively charged nitrogens in MV^{2+} with the negatively charged sulfurs on the S-terminated stoichiometric lattice.

CONCLUSIONS

In summary, we have described the surface composition-dependent binding of methyl viologen (MV^{2+}) to CdS QDs that are synthetically enriched to various degrees with either Cd or S at their surfaces. The surfaces of CdS QDs can be controlled synthetically, *via* injection of excess precursor during the final growth stage, or through a simple dilution of the QDs to remove weakly bound Cd-OA postsynthesis. The

efficiency with which MV^{2+} quenches the PL of these QDs through photoinduced electron transfer depends on the binding affinity of MV^{2+} for their surfaces. Fits of the PL quenching curves for both Cd-enriched and S-enriched QDs with a model that relates the PL intensity of the ensemble to the distribution of MV^{2+} adsorbed in electron transfer-active geometries reveals two general mechanisms by which MV^{2+} adsorbs to the QD surface for all samples studied: (i) adsorption to stoichiometric CdS surfaces through displacement of weakly bound Cd-OA complexes from the QD surface (with displacement constant $K_{a,1} = 3.5 \times 10^3\ M^{-1}$), and (ii) direct adsorption to exposed stoichiometric CdS surfaces (with adsorption constant $K_{a,2} = 1.5 \times 10^5\ M^{-1}$). The relative importance of these two mechanisms depends on the surface chemistry of the QDs. The fact that both mechanisms lead to adsorption of MV^{2+} onto a stoichiometric CdS surface is consistent with our measurement, by transient absorption, that photoinduced electron transfer from the QD to MV^{2+} occurs with very similar rate constants for Cd-enriched and S-enriched QDs ($\sim 2 \times 10^{10}\ s^{-1}$). *Ab initio* calculations suggest that MV^{2+} adsorbs with its bipyridyl core lying flat on the QD surface and prefers a S-terminated stoichiometric surface (over a Cd-terminated surface) because of the favorable interaction of the electron-poor nitrogens on MV^{2+} with electron-rich sulfur ions.

Historically, the details of electron transfer mechanisms within organic donor–acceptor pairs have been elucidated best when the geometry of the donor–acceptor pair is known precisely, either through structural measurements (for example, the supramolecular systems that compose photosynthetic reaction centers)[52] or through control of that geometry with rigid covalent linkers between redox moieties.[53] The complexity of the QD surface makes obtaining this precise knowledge and control more difficult than in organic systems, especially when, as in the case of MV^{2+}-QD complexes, the QD and its redox partner are linked by electrostatic or van der Waals interactions rather than a well-defined coordinate or covalent bond. We believe this work shows, however, that this complexity can be managed, and important physical conclusions and quantitative results can be derived, with well-defined models for distribution of molecules on the QD surfaces, and with a set of experimental systems with carefully designed, well-characterized variations in the surface structure of the QDs. QDs offer many well-documented advantages for solar energy conversion to electricity and fuels,[54,55] but the creation of functional hybrid materials for complex reactions like photocatalysis depends critically on the details of interfacial structure and processes.

EXPERIMENTAL METHODS

Ground State Absorption and Emission. We collect ground state absorption spectra on samples in 2-mm glass cuvettes with a Varian Cary 5000 and baseline-correct the spectra by subtracting the absorption spectrum of neat solvent from all samples. We perform photoluminescence (PL) experiments of samples in 2-mm quartz cuvettes on a Horiba Fluorolog-3 spectrofluorometer in the front-face geometry, with excitation and emission slit widths of 3 nm. Unless otherwise noted, we pump the samples at 400 nm and divide the resulting PL spectra by the instantaneous intensity of the excitation lamp at all wavelengths. For samples containing MV^{2+}, we add methanolic solutions of MV^{2+} to clean scintillation vials and evaporate the solvent before adding CdS QDs in THF.

X-ray Photoelectron Spectroscopy (XPS). We prepared samples for XPS by drop-casting solutions of QDs in THF onto Si/SiO_2 wafers immediately before loading the sample into the XPS vacuum chamber. We collect XPS spectra on a Thermo Scientific ESCALAB 250 Xi spectrometer, using an aluminum anode (1486.6 eV) at 225 W. We use a dwell time of 100 ms and collect 3 scans of C and O and 10 scans of Cd and S for each sample. All spectra are normalized in energy to the C1s peak.

Nuclear Magnetic Resonance (NMR). We perform ^1H NMR on a Bruker Ag500 spectrometer. We prepare NMR samples by evaporating the solvent under light heat and vacuum, washing the collected QD film several times with acetone, and pulling vacuum on the resulting film to remove residual volatile organics. We then dissolve the QDs in $CDCl_3$ (99.8 atom % D) with 0.2 wt % biphenyl added as an internal concentration standard and confirm the concentration using the optical absorbance peak of biphenyl at 250 nm.

Transient Absorption Spectroscopy (TA). Our transient absorption (TA) setup is described in detail elsewhere.[9,56] We collect picosecond-to-nanosecond TA measurements in the visible and near-infrared (NIR) spectral regions on a commercial HELIOS spectrometer, and nanosecond-to-microsecond measurements in the visible and NIR regions on a commercial EOS spectrometer. We pump the solutions, in 2-mm cuvettes containing a Teflon stir bar, at 400 nm under constant stirring to avoid local heating and buildup of charge. We measured the total instrument response function to be ~300 fs.

Conflict of Interest: The authors declare no competing financial interest.

Acknowledgment. Research was funded in part by the ANSER Center, an Energy Frontier Research Center funded by the U.S. Department of Energy, Office of Science, Office of Basic Energy Sciences, under Award No. DE-SC0001059 (synthesis of materials and optical spectroscopy), and by a postdoctoral fellowship to S.C.J. from the International Institute of Nanotechnology (IIN) at Northwestern (calculations). D.J.W. (ultrafast spectroscopy) is supported by the Department of Energy Office of Science Graduate Fellowship Program (DOE SCGF), made possible in part by the American Recovery and Reinvestment Act of 2009, administered by ORISE-ORAU under Contract DE-AC0506OR23100. The authors thank Martin R. McPhail and Kedy Edme for performing preliminary NMR experiments on the QD samples.

Supporting Information Available: Sample characterization, experimental details, and additional results, including Figures S1–S9. This material is available free of charge *via* the Internet at http://pubs.acs.org.

REFERENCES AND NOTES

1. Rabaey, K.; Rozendal, R. A. Microbial Electrosynthesis—Revisiting the Electrical Route for Microbial Production. *Nat. Rev. Microbiol.* **2010**, *8*, 706–716.
2. Krishnan, V. V.; Dokoutchaev, A. G.; Thompson, M. E. Direct Production of Hydrogen Peroxide with Palladium Supported on Phosphate Viologen Phosphonate Catalysts. *J. Catal.* **2000**, *196*, 366–374.

3. Meisel, D.; Mulac, W.; Matheson, M. Catalysis of Methyl Viologen Radical Reactions by Polymer-Stabilized Gold Sols. *J. Phys. Chem.* **1981**, *85*, 179–187.
4. DiCosimo, R.; Wong, C.-H.; Daniels, L.; Whitesides, G. M. Enzyme-Catalyzed Organic Synthesis: Electrochemical Regeneration of Nad(P)H from Nad(P) Using Methyl Viologen and Flavoenzymes. *J. Org. Chem.* **1981**, *46*, 4622–4623.
5. Jiang, Z.-J.; Kelley, D. F. Hot and Relaxed Electron Transfer from the CdSe Core and Core/Shell Nanorods. *J. Phys. Chem. C* **2011**, *115*, 4594–4602.
6. Zhu, H.; Lian, T. Enhanced Multiple Exciton Dissociation from CdSe Quantum Rods: The Effect of Nanocrystal Shape. *J. Am. Chem. Soc.* **2012**, *134*, 11289–11297.
7. Zhu, H.; Song, N.; Rodríguez-Córdoba, W.; Lian, T. Wave Function Engineering for Efficient Extraction of up to Nineteen Electrons from One CdSe/CdS Quasi-Type II Quantum Dot. *J. Am. Chem. Soc.* **2012**, *134*, 4250–4257.
8. Matylitsky, V. V.; Dworak, L.; Breus, V. V.; Basché, T.; Wachtveitl, J. Ultrafast Charge Separation in Multiexcited Cdse Quantum Dots Mediated by Adsorbed Electron Acceptors. *J. Am. Chem. Soc.* **2009**, *131*, 2424–2425.
9. Morris-Cohen, A. J.; Frederick, M. T.; Cass, L. C.; Weiss, E. A. Simultaneous Determination of the Adsorption Constant and the Photoinduced Electron Transfer Rate for a Cds Quantum Dot−Viologen Complex. *J. Am. Chem. Soc.* **2011**, *133*, 10146–10154.
10. Morris-Cohen, A. J.; Peterson, M. D.; Frederick, M. T.; Kamm, J. M.; Weiss, E. A. Evidence for a Through-Space Pathway for Electron Transfer from Quantum Dots to Carboxylate-Functionalized Viologens. *J. Phys. Chem. Lett.* **2012**, *3*, 2840–2844.
11. Tisdale, W. A.; Williams, K. J.; Timp, B. A.; Norris, D. J.; Aydil, E. S.; Zhu, X.-Y. Hot-Electron Transfer from Semiconductor Nanocrystals. *Science* **2010**, *328*, 1543–1547.
12. Boulesbaa, A.; Issac, A.; Stockwell, D.; Huang, Z.; Huang, J.; Guo, J.; Lian, T. Ultrafast Charge Separation at CdS Quantum Dot/Rhodamine B Molecule Interface. *J. Am. Chem. Soc.* **2007**, *129*, 15132–15133.
13. Nitzan, A. *Chemical Dynamics in Condensed Phases: Relaxation, Transfer, and Reactions in Condensed Molecular Systems*; Oxford University Press: New York, 2006.
14. Moreels, I.; Fritzinger, B.; Martins, J. C.; Hens, Z. Surface Chemistry of Colloidal PbSe Nanocrystals. *J. Am. Chem. Soc.* **2008**, *130*, 15081–15086.
15. Anderson, N. C.; Hendricks, M. P.; Choi, J. J.; Owen, J. S. Ligand Exchange and the Stoichiometry of Metal Chalcogenide Nanocrystals: Spectroscopic Observation of Facile Metal-Carboxylate Displacement and Binding. *J. Am. Chem. Soc.* **2013**, 18536–18548.
16. Moreels, I.; Lambert, K.; De Muynck, D.; Vanhaecke, F.; Poelman, D.; Martins, J. C.; Allan, G.; Hens, Z. Composition and Size-Dependent Extinction Coefficient of Colloidal PbSe Quantum Dots. *Chem. Mater.* **2007**, *19*, 6101–6106.
17. Jasieniak, J.; Mulvaney, P. From Cd-Rich to Se-Rich-the Manipulation of CdSe Nanocrystal Surface Stoichiometry. *J. Am. Chem. Soc.* **2007**, *129*, 2841–2848.
18. Taylor, J.; Kippeny, T.; Rosenthal, S. J. Surface Stoichiometry of CdSe Nanocrystals Determined by Rutherford Backscattering Spectroscopy. *J. Cluster Sci.* **2001**, *12*, 571–582.
19. Morris-Cohen, A. J.; Frederick, M. T.; Lilly, G. D.; McArthur, E. A.; Weiss, E. A. Organic Surfactant-Controlled Composition of the Surfaces of CdSe Quantum Dots. *J. Phys. Chem. Lett.* **2010**, *1*, 1078–1081.
20. Dai, Q.; Wang, Y.; Li, X.; Zhang, Y.; Pellegrino, D. J.; Zhao, M.; Zou, B.; Seo, J.; Wang, Y.; Yu, W. W. Size-Dependent Composition and Molar Extinction Coefficient of PbSe Semiconductor Nanocrystals. *ACS Nano* **2009**, *3*, 1518–1524.
21. Subila, K.; Kishore Kumar, G.; Shivaprasad, S. M.; George Thomas, K. Luminescence Properties of CdSe Quantum Dots: Role of Crystal Structure and Surface Composition *J. Phys. Chem. Lett.* **2013**, 2774–2779.
22. Owen, J. S.; Park, J.; Trudeau, P.-E.; Alivisatos, A. P. Reaction Chemistry and Ligand Exchange at Cadmium−Selenide Nanocrystal Surfaces. *J. Am. Chem. Soc.* **2008**, *130*, 12279–12281.
23. Morris-Cohen, A. J.; Donakowski, M. D.; Knowles, K. E.; Weiss, E. A. The Effect of a Common Purification Procedure on the Chemical Composition of the Surfaces of CdSe Quantum Dots Synthesized with Trioctylphosphine Oxide. *J. Phys. Chem. C* **2009**, *114*, 897–906.
24. Hughes, B. K.; Ruddy, D. A.; Blackburn, J. L.; Smith, D. K.; Bergren, M. R.; Nozik, A. J.; Johnson, J. C.; Beard, M. C. Control of PbSe Quantum Dot Surface Chemistry and Photophysics Using an Alkylselenide Ligand. *ACS Nano* **2012**, *6*, 5498–5506.
25. Omogo, B.; Aldana, J. F.; Heyes, C. D. Radiative and Nonradiative Lifetime Engineering of Quantum Dots in Multiple Solvents by Surface Atom Stoichiometry and Ligands. *J. Phys. Chem. C* **2013**, *117*, 2317–2327.
26. Oh, S. J.; Berry, N. E.; Choi, J.-H.; Gaulding, E. A.; Paik, T.; Hong, S.-H.; Murray, C. B.; Kagan, C. R. Stoichiometric Control of Lead Chalcogenide Nanocrystal Solids to Enhance Their Electronic and Optoelectronic Device Performance. *ACS Nano* **2013**, *7*, 2413–2421.
27. Wei, H. H.-Y.; Evans, C. M.; Swartz, B. D.; Neukirch, A. J.; Young, J.; Prezhdo, O. V.; Krauss, T. D. Colloidal Semiconductor Quantum Dots with Tunable Surface Composition. *Nano Lett.* **2012**, *12*, 4465–4471.
28. Soni, U.; Sapra, S. The Importance of Surface in Core−Shell Semiconductor Nanocrystals. *J. Phys. Chem. C* **2010**, *114*, 22514–22518.
29. Nag, A.; Kovalenko, M. V.; Lee, J.-S.; Liu, W.; Spokoyny, B.; Talapin, D. V. Metal-Free Inorganic Ligands for Colloidal Nanocrystals: S^{2-}, HS^{-}, Se^{2-}, HSe^{-}, Te^{2-}, HTe^{-}, TeS_3^{2-}, OH^{-}, and NH_2^{-} as Surface Ligands. *J. Am. Chem. Soc.* **2011**, *133*, 10612–10620.
30. Yu, W. W.; Qu, L.; Guo, W.; Peng, X. Experimental Determination of the Extinction Coefficient of CdTe, CdSe, and CdS Nanocrystals. *Chem. Mater.* **2003**, *15*, 2854–2860.
31. Hässelbarth, A.; Eychmüller, A.; Weller, H. Detection of Shallow Electron Traps in Quantum Sized CdS by Fluorescence Quenching Experiments. *Chem. Phys. Lett.* **1993**, *203*, 271–276.
32. Jones, M.; Nedeljkovic, J.; Ellingson, R. J.; Nozik, A. J. Rumbles, G. Photoenhancement of Luminescence in Colloidal CdSe Quantum Dot Solutions. *J. Phys. Chem. B* **2003**, *107*, 11346–11352.
33. Mooney, J.; Krause, M. M.; Saari, J. I.; Kambhampati, P. Challenge to the Deep-Trap Model of the Surface in Semiconductor Nanocrystals. *Phys. Rev. B* **2013**, *87*, 081201/01–081201/05.
34. Krause, M. M.; Mooney, J.; Kambhampati, P. Chemical and Thermodynamic Control of the Surface of Semiconductor Nanocrystals for Designer White Light Emitters. *ACS Nano* **2013**, *7*, 5922–5929.
35. Klimov, V.; Bolivar, P. H.; Kurz, H. Ultrafast Carrier Dynamics in Semiconductor Quantum Dots. *Phys. Rev. B* **1996**, *53*, 1463–1467.
36. Ren, S.-Y.; Ren, S.-F. Total and Surface Density of States in CdS Semiconductor Clusters. *J. Phys. Chem. Solids* **1998**, *59*, 1327–1330.
37. Collins, R. Mechanism and Defect Responsible for Edge Emission in CdS. *J. Appl. Phys.* **1959**, *30*, 1135–1140.
38. Nanda, J.; Kuruvilla, B. A.; Sarma, D. D. Photoelectron Spectroscopic Study of CdS Nanocrystallites. *Phys. Rev. B* **1999**, *59*, 7473–7479.
39. Meissner, D.; Benndorf, C.; Memming, R. Photocorrosion of Cadmium Sulfide: Analysis by Photoelectron Spectroscopy. *Appl. Surf. Sci.* **1987**, *27*, 423–436.
40. Winkler, U.; Eich, D.; Chen, Z.; Fink, R.; Kulkarni, S.; Umbach, E. Detailed Investigation of CdS Nanoparticle Surfaces by High-Resolution Photoelectron Spectroscopy. *Chem. Phys. Lett.* **1999**, *306*, 95–102.
41. Tibbetts, G. G.; Burkstrand, J. M. Auger and Photoelectron Study of Codeposited Sulfur and Oxygen Layers on Silver (111). *J. Vac. Sci. Technol.* **1978**, *15*, 497–501.
42. Lichtensteiger, M.; Webb, C.; Lagowski, J. Electron Stimulated Adsorption: Surface Activation and Preferential Binding of Oxygen to Sulfur on Cds. *Surf. Sci.* **1980**, *97*, L375–L379.

43. Morris-Cohen, A. J.; Vasilenko, V.; Amin, V. A.; Reuter, M. G.; Weiss, E. A. Model for Adsorption of Ligands to Colloidal Quantum Dots with Concentration-Dependent Surface Structure. *ACS Nano* **2011**, *6*, 557–565.
44. Huang, J.; Huang, Z.; Jin, S.; Lian, T. Exciton Dissociation in CdSe Quantum Dots by Hole Transfer to Phenothiazine *J. Phys. Chem. C* **2008**, *112*, 19734–19738.
45. Tachiya, M. Kinetics of Quenching of Luminescent Probes in Micellar Systems. II. *J. Chem. Phys.* **1982**, *76*, 340–348.
46. Kopping, J. T.; Patten, T. E. Identification of Acidic Phosphorus-Containing Ligands Involved in the Surface Chemistry of CdSe Nanoparticles Prepared in Tri-*N*-Octylphosphine Oxide Solvents. *J. Am. Chem. Soc.* **2008**, *130*, 5689–5698.
47. McPhail, M. R.; Weiss, E. A. The Role of Alkyl-Sulfur Adducts in the Growth and Final Surface Chemistry of PbS Quantum Dots. Submitted.
48. Li, Z.; Ji, Y.; Xie, R.; Grisham, S. Y.; Peng, X. Correlation of CdS Nanocrystal Formation with Elemental Sulfur Activation and Its Implication in Synthetic Development. *J. Am. Chem. Soc.* **2011**, *133*, 17248–17256.
49. Bateman, L.; Moore, C.; Porter, M. The Reaction of Sulfur and Sulfur Compounds with Olefinic Substances. Part Xi. The Mechanism of Interaction of Sulfur with Mono-Olefins and 1,5-Dienes. *Rubber Chem. Technol.* **1958**, *31*, 1090–1104.
50. Coronado, J. M.; Zorn, M. E.; Tejedor-Tejedor, I.; Anderson, M. A. Photocatalytic Oxidation of Ketones in the Gas Phase over TiO_2 Thin Films: A Kinetic Study on the Influence of Water Vapor. *Appl. Catal., B* **2003**, *43*, 329–344.
51. Vorontsov, A. V.; Kurkin, E. N.; Savinov, E. N. Study of TiO_2 Deactivation During Gaseous Acetone Photocatalytic Oxidation. *J. Catal.* **1999**, *186*, 318–324.
52. Nakagawa, H.; Okada, T.; Koyama, Y. Role of Amino-Acid Sidechains in Electron-Transfer Reactions in Reaction Center of Rhodopseudomonas Viridis as Revealed by Extended Hückel Molecular Orbital Calculations. *Biospectroscopy* **1995**, *1*, 169–185.
53. Wasielewski, M. R. Photoinduced Electron Transfer in Supramolecular Systems for Artificial Photosynthesis. *Chem. Rev. (Washington, DC, U. S.)* **1992**, *92*, 435–461.
54. Semonin, O. E.; Luther, J. M.; Choi, S.; Chen, H.-Y.; Gao, J.; Nozik, A. J.; Beard, M. C. Peak External Photocurrent Quantum Efficiency Exceeding 100% *via* MEG in a Quantum Dot Solar Cell. *Science* **2011**, *334*, 1530–1533.
55. Nozik, A. Quantum Dot Solar Cells. *Phys. E (Amsterdam, Neth.)* **2002**, *14*, 115–120.
56. McArthur, E. A.; Morris-Cohen, A. J.; Knowles, K. E.; Weiss, E. A. Charge Carrier Resolved Relaxation of the First Excitonic State in CdSe Quantum Dots Probed with Near-Infrared Transient Absorption Spectroscopy. *J. Phys. Chem. B* **2010**, *114*, 14514–14520.